

EXPLORING THE PROPERTIES OF CHOKED GAMMA-RAY BURSTS WITH ICECUBE’S HIGH ENERGY NEUTRINOS

PETER B. DENTON¹ AND IRENE TAMBORRA^{1,2}

¹ Niels Bohr International Academy, Niels Bohr Institute, University of Copenhagen, Blegdamsvej 17, 2100, Copenhagen, Denmark

² DARK, Niels Bohr Institute, University of Copenhagen, Juliane Maries Vej 30, 2100, Copenhagen, Denmark

Draft version March 6, 2018

ABSTRACT

Long duration gamma-ray bursts (GRBs) have often been considered as the natural evolution of some core-collapse supernova (CCSN) progenitors. However, the fraction of CCSNe linked to astrophysical jets and their properties are still poorly constrained. While any successful astrophysical jet harbored in a CCSN should produce high energy neutrinos, photons may be able to successfully escape the stellar envelope only for a fraction of progenitors, possibly leading to the existence of high-luminosity, low-luminosity and not-electromagnetically bright (“choked”) GRBs. By postulating a CCSN–GRB connection, we accurately model the jet physics within the internal-shock GRB model and assume scaling relations for the GRB parameters that depend on the Lorentz boost factor Γ . The IceCube high energy neutrino flux is then employed as an upper limit of the neutrino background from electromagnetically bright and choked GRBs to constrain the jet and the progenitor properties. The current IceCube data set is compatible with up to 1% of all CCSNe harboring astrophysical jets. Interestingly, those jets are predominantly choked. Our findings suggest that neutrinos can be powerful probes of the burst physics and can provide major insights on the CCSN–GRB connection.

Keywords: gamma-ray burst: general — supernovae: general — neutrinos

1. INTRODUCTION

Gamma ray bursts (GRBs) are among the most energetic astrophysical transients (Mészáros 2006; Kumar & Zhang 2014; Mészáros 2017). GRBs are expected to be sources of high energy neutrinos produced through hadronic and lepto-hadronic interactions. Neutrinos from GRBs could be possibly detected by neutrino telescopes. However, targeted searches of neutrinos from high-luminosity GRBs (HL-GRBs) have reported evidence for a lack of statistically significant spatial and timing correlation of neutrino data (Schmid & Turpin 2016; Aartsen et al. 2017b) constraining the proposed theoretical models (Baerwald et al. 2012; He et al. 2012; Bartos et al. 2013).

At the same time, a flux of astrophysical neutrinos has been detected by the IceCube Neutrino Observatory (Aartsen et al. 2013b,a, 2014, 2015b,a,c,d). While the flux is held to be predominantly extragalactic (Palladino & Vissani 2016; Denton et al. 2017; Aartsen et al. 2017a), its origin is currently unknown. In this context, “choked” GRBs (see e.g. Mészáros & Waxman (2001); Ando & Beacom (2005)) have been considered as possible sources of some of the IceCube neutrinos (Murase & Ioka 2013; Tamborra & Ando 2016, 2015; Senno et al. 2016; Murase et al. 2016; Senno et al. 2017).

A choked jet is one where the jet is successful in accelerating particles, but electromagnetic radiation is unsuccessful in escaping the stellar envelope. Choked GRBs may even be more abundant than the GRBs ordinarily observed in photons (Mészáros & Waxman 2001; Razzaque et al. 2003a, 2004, 2003b; Ando & Beacom 2005; Horiuchi & Ando 2008; Murase & Ioka 2013). Neutrinos and possibly gravitational waves may be the only messengers from these sources.

There is solid evidence that GRBs and core-collapse supernovae (CCSNe) are related (Paczynski 1998; Hjorth & Bloom 2012; Modjaz 2011; Hjorth 2013; Margutti et al. 2014; Sobacchi et al. 2017; Lazzati et al. 2012). This was also fore-

seen in the so-called collapsar model (MacFadyen & Woosley 1999; MacFadyen et al. 2001; Woosley & Bloom 2006) and is supported by the fact that we expect a comparable amount of energy to be released in CCSNe and GRBs. Recent work, see e.g. Sobacchi et al. (2017), suggests that possibly a large fraction of jets harbored in CCSNe might not be electromagnetically visible. In this work, we take the CCSN–GRB relationship seriously and investigate a model of astrophysical jets originating from CCSNe.

We build up a model where the same physics applies in jets that produce γ -rays and those that do not when the jet is trapped within the stellar envelope. According to our scenario, one could think of high (HL)- and low-luminosity (LL)- GRBs as sub-classes of one larger ensemble to which choked GRBs also belong (Bromberg et al. 2011a; Nakar 2015). Early literature (Murase et al. 2006; Gupta & Zhang 2007; Liu et al. 2011; Liu & Wang 2013; Murase & Ioka 2013; Tamborra & Ando 2016, 2015) proved that the neutrino production from LL- and choked GRBs can even be larger than the one expected for ordinary GRBs.

We explore a general model where the jet properties scale as a function of the Lorentz boost factor Γ and estimate the total diffuse neutrino background from both bright and choked jets, by linking choked GRBs with observed GRBs under the same model. To do this, we perform detailed simulations within the internal-shock GRB model and vary the jet parameters to provide a realistic picture of the diffuse flux from the whole jet population. We include both pp and $p\gamma$ interactions as well as all relevant cooling processes for protons and intermediate accelerated particles and adopt energy-dependent cross sections for all cooling processes relevant to our purpose.

For the sake of completeness, we distinguish among two GRB models. The first one is a “simple” GRB model that is based on the commonly used scaling law $\theta_j = 1/\Gamma$ applied to the whole jet, with θ_j being the half opening angle; in this model Γ varies across the GRB population. The second one is an “advanced” GRB model which contains a Γ -dependent

GRB population distribution as does the simple model, but also contains a distribution of Γ within the jet. Finally, we use IceCube data to define upper limits on the jet energy and the fraction of CCSNe that form jets.

The outline of the paper is as follows. In Sec. 2, we first review standard jet physics and explain how each jet parameter is related to the others. We then calculate the flux as seen at Earth. We introduce the simple GRB model in Sec. 3 and calculate the diffuse intensity normalized to the CCSN and HL-GRB rates. The advanced GRB model is presented in Sec. 4. Then we compare the predicted diffuse intensities within the two GRB models to IceCube's data in Sec. 5 and discuss our findings in Sec. 6. Our conclusions are reported in Sec. 7.

2. HIGH ENERGY NEUTRINO PRODUCTION IN ASTROPHYSICAL JETS

In this Section, we will overview the properties of the astrophysical jets and discuss the relevant cooling processes affecting the protons and secondary particles. We will then convert those jet properties into the diffuse neutrino intensity observed at the Earth. For simplicity, we will now rely on the simple GRB model, wherein each jet is described by a single value of Γ , until otherwise specified.

2.1. Properties of the Astrophysical Jet

We parameterize the astrophysical jet by the amount of kinetic energy in the jet \tilde{E}_j , bulk Lorentz factor Γ , and electron (magnetic) energy fraction ϵ_e (ϵ_B). There are various internal properties that are functions of jet parameters. We enumerate them here for reference.

First, we take the standard theoretical $\Gamma - \theta_j$ relation from special relativity, $\theta_j = 1/\Gamma$ (see, e.g., Mészáros (2006)). This form is often used throughout the literature with the argument that given a Lorentz boost factor Γ , the typical angular scale is $\theta_j = 1/\Gamma$. We hereby adopt a modified version of this $\Gamma - \theta_j$ relation to match observed jet angles:

$$\theta_j = \begin{cases} \frac{1}{\Gamma} & \Gamma \leq 100 \\ \frac{30}{\Gamma} & \Gamma > 100 \end{cases} \quad (1)$$

The above relation for a typical HL-GRB with $\Gamma = 300$ gives an opening angle of $\theta_j = 6^\circ$, consistent with observations (Goldstein et al. 2016). The break at $\Gamma = 100$ is taken from Cenko et al. (2011); Ackermann et al. (2011); Dermer et al. (2014); Tamborra & Ando (2015). Measurements of the jet opening angle for LL-GRBs are more uncertain. Nevertheless, for the range $\Gamma \in [3, 100]$ the opening angle varies in the range $\theta_j \in [0.6^\circ, 19^\circ]$ which is consistent with estimations of LL-GRBs jet opening angle reported in the literature (Toma et al. 2007; Liang et al. 2007; Daigne & Mochkovitch 2007; Bromberg et al. 2011a; Zhang et al. 2012; Nakar 2015).

The magnetic field strength is given by,

$$\frac{B'^2}{8\pi} = 4\epsilon_B \frac{E'_j}{V'}, \quad (2)$$

where the jet volume is given by,

$$V' = \Omega_j \tilde{r}_j^2 c \tilde{t}_j \Gamma. \quad (3)$$

Note that we distinguish among three reference frames: X - Earth, \tilde{X} - star, X' - jet. Energies in each frame are related by $\tilde{E} = (1+z)E$, and $\tilde{E} = \Gamma E'$. Times are related by $t = (1+z)\tilde{t}$, and $t' = \Gamma\tilde{t}$. Luminosities are related by $\tilde{L} = (1+z)^2 L$. The solid angle for both jets is,

$$\Omega_j = 4\pi(1 - \cos \theta_j) \approx 2\pi\theta_j^2. \quad (4)$$

The internal-shock radius \tilde{r}_j is defined as

$$\tilde{r}_j = 2c\tilde{t}_v\Gamma^2. \quad (5)$$

The jet variability time is taken from an empirical fit to HL-GRBs (Sonbas et al. 2015) and a maximum to cap the variability time for LL-GRBs,

$$\tilde{t}_v = \min(2.8 \times 10^9 \Gamma^{-4.05}, 100) \text{ s}, \quad (6)$$

which breaks at $\Gamma = 69$. While variability time measurements of LL-GRBs are sparse, GRB060218/SN2006aj measured by Swift had a variability time of ~ 200 s, so taking $\tilde{t}_v \sim 100$ s as an upper limit for low Γ jets is reasonable (Campana et al. 2006; Gupta & Zhang 2007). The comoving photon, electron, and proton densities are,

$$n'_\gamma = \frac{4E'_j\epsilon_e}{V'E'_{\gamma,b}}, \quad n'_e \simeq n'_p = \frac{E'_j}{V'm_p c^2}, \quad (7)$$

where we have taken the comoving electron density as essentially the same as the comoving proton density. The photon break energy $E'_{\gamma,b}$ is defined in Sec. 2.4.

For the jet duration \tilde{t}_j , we use a power law relation to describe both longer GRBs with lower Γ 's and shorter GRBs with higher Γ 's. Then, $\tilde{t}_j \propto 1/\Gamma$ normalized to $\tilde{t}_j = 10$ s at $\Gamma = 300$ (Gehrels & Razzaque 2013; Lü et al. 2017).

2.2. Conditions to Successfully Accelerate Particles in the Jet

As was pointed out in Murase & Ioka (2013), if the jet density is too high, then the velocity gain in each shock of protons will not be enough to reach canonical Fermi acceleration and the jet will never accelerate particles to high energy. To ensure that a jet is successful in accelerating protons, we introduce the optical depth of the jet (given by the Thomson optical depth),

$$\tau'_T = \frac{\sigma_T n'_p \tilde{r}_j}{\Gamma}, \quad (8)$$

and apply the conservative constraint $\tau'_T \lesssim 1$. Jets that do not meet this constraint are considered unsuccessful and no particles are created in these jets.

Separate from the issue of whether or not a jet is successful at accelerating protons, we also determine if a jet is choked or not. A choked jet is one in which the jet head does not escape the stellar envelope. Under the assumption that the jet becomes collimated, we use the following definition for the jet head radius (Bromberg et al. 2011b),

$$\tilde{r}_h = 5.4 \times 10^{10} \text{ cm } \tilde{t}_{j,1}^{6/5} \tilde{L}_{\text{iso},52}^{2/5} \times \left(\frac{\theta_j}{0.2}\right)^{-8/5} \left(\frac{M_*}{20 M_\odot}\right)^{-2/5} R_{*,11}^{1/5}, \quad (9)$$

and estimate it for a typical Wolf-Rayet star with mass $M_* = 20 M_\odot$ and radius $R_* = R_\odot$. The isotropic luminosity is $\tilde{L}_{\text{iso}} = 4\pi\tilde{E}_j/\tilde{t}_j\Omega_j$. Since many of the parameters in Eq. 9 scale with Γ , we note that the overall Γ and \tilde{E}_j dependence of the jet head radius is $\tilde{r}_h \propto \tilde{E}_j^{2/5}\Gamma^{8/5}$. We here use the standard notation, $Q_x = Q/10^x$ in cgs units, unless otherwise specified. The condition for a jet to be choked in photons is when $\tilde{r}_h < R_*$. If the internal shock radius is larger than the stellar radius then no cocoon can form and the jet is not collimated. In this case, Eq. 9 no longer applies as there is no jet head since the jet is visible (not choked).

2.3. Particle Acceleration and Cooling Processes

All of the charged particles in the jet, protons, pions, kaons, and muons lose energy to various processes. To determine the final spectrum of neutrinos, the cooling process of each particle needs to be determined. In different regimes of energy and Γ , as well as the other parameters, different cooling processes dominate.

2.3.1. Protons

Protons are accelerated on a time scale given by the magnetic field strength,

$$t'_{p,acc} = \frac{E'_p}{B'ec}. \quad (10)$$

Protons continue to be accelerated until they lose energy faster than their acceleration time scale. The energy loss mechanisms that they may suffer are listed in the following equations. Protons lose energy to synchrotron losses in magnetic field,

$$t'_{p,sync} = \frac{3m_p^4 c^3 8\pi}{4\sigma_T m_e^2 E'_p B'^2}, \quad (11)$$

where $\sigma_T = 6.65 \times 10^{-25} \text{ cm}^2$ is the Thomson cross section. Protons are cooled by inverse Compton scattering, which we split into two regimes,

$$t'_{p,IC} = \begin{cases} \frac{3m_p^4 c^3}{4\sigma_T m_e^2 E'_p E'_\gamma n'_\gamma} & E'_p E'_\gamma < m_p^2 c^4 \\ \frac{3E'_p E'_\gamma}{4\sigma_T m_e^2 c^5 n'_\gamma} & E'_p E'_\gamma > m_p^2 c^4 \end{cases}. \quad (12)$$

The Bethe-Heitler process ($p\gamma \rightarrow pe^+e^-$) has a cooling time of,

$$t'_{p,BH} = \frac{E'_p \sqrt{m_p^2 c^4 + 2E'_p E'_\gamma}}{2n'_\gamma \sigma_{BH} m_e c^3 (E'_p + E'_\gamma)}, \quad (13)$$

where σ_{BH} is,

$$\sigma_{BH} = \alpha r_e^2 \left[\frac{28}{9} \ln \left(\frac{2E'_p E'_\gamma}{m_p m_e c^4} \right) - \frac{106}{9} \right]. \quad (14)$$

with α being the fine structure constant and r_e the classical electron radius. Protons are also cooled via $p\gamma$ and pp interactions. Their cooling times are,

$$t'_{p,p\gamma} = \frac{E'_p}{c\sigma_{p\gamma} n'_\gamma \Delta E'_p} \quad (15)$$

$$t'_{p,pp} = \frac{E'_p}{c\sigma_{pp} n'_p \Delta E'_p}, \quad (16)$$

with $\Delta E'_p/E'_p = 0.2, 0.8$ for the $p\gamma, pp$ cases respectively. Energy dependent cross sections, $\sigma_{p\gamma}$ and σ_{pp} , are taken from (Patrignani et al. 2016)¹. Finally, protons lose energy due to adiabatic cooling from the expansion of the jet,

$$t'_{p,ac} = \frac{\tilde{r}_j}{c\Gamma}. \quad (17)$$

Together, the inverse of the total cooling for protons is the sum of the inverses of each individual cooling time, $t'^{-1}_{p,c} =$

¹ For low energies ($\sqrt{s} < 10 \text{ GeV}$, with s being the Mandelstam variable), the PDG data are used, while the $\ln^2 s$ parameterization is used for high energy interactions.

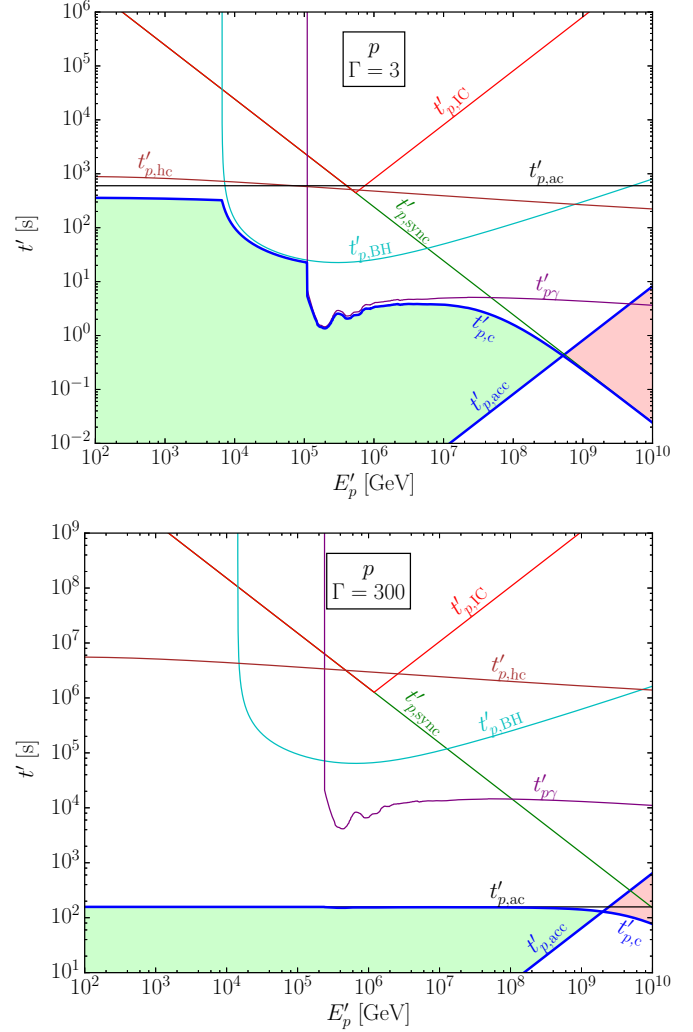


Figure 1. Cooling processes for protons as a function of proton energy in the comoving frame for $\Gamma = 3$ (top) and $\Gamma = 300$ (bottom) for the simple GRB model. The jet energy is fixed to $\tilde{E}_j = 10^{51} \text{ erg}$, the energy fractions are $\epsilon_e = \epsilon_B = 0.1$, and the redshift is $z = 1$. The thin solid lines mark the various individual cooling processes; the tick solids line are the total cooling, and the acceleration time. The green shaded region on the left of each figure shows the largely uncooled portion of the spectrum, while the red region on the right shows the cooled portion of the spectrum.

$\sum_i t'^{-1}_{p,i}$. The cooled proton spectrum is the uncooled spectrum scaled by an additional factor of $[1 - \exp(-\eta_p)]$, where the number of energy losses is, $\eta_p = t'_{p,c}/t'_{p,acc}$.

Figure 1 shows the cooling times for protons from each process for our canonical high- and low- Γ bursts as a function of the proton energy for jet energy $\tilde{E}_j = 10^{51} \text{ erg}$, energy fractions $\epsilon_e = \epsilon_B = 0.1$, and redshift $z = 1$. The solid lines mark the various cooling processes, while the dash-dotted line represents the total cooling, and the dotted line is the acceleration time.

2.3.2. Intermediate Particles

Pions and kaons created in $p\gamma$ and pp interactions decay into a muon neutrino and muons. The muons subsequently decay into a muon neutrino and an electron neutrino (and an

Table 1

Ratios for different intermediate processes. a_i relates the energy of the parent proton to the energy of the resultant neutrino through a given channel, $E_{\nu,i} = a_i E_p$. N_i is the energy that goes to neutrinos from one $p\gamma$ interaction; the first number in the product is the percentage of $p\gamma$ interactions that go to π , K , and the next two numbers are the amount of energy that remain from proton to intermediate and then intermediate to neutrino.

	π	μ_π	K	μ_K
a_i	$\frac{1}{5} \cdot \frac{1}{4}$	$\frac{1}{5} \cdot \frac{3}{4} \cdot \frac{1}{3}$	$\frac{1}{5} \cdot \frac{1}{2}$	$\frac{1}{5} \cdot \frac{1}{2} \cdot \frac{1}{3}$
N_i	$0.97 \cdot \frac{1}{4} \cdot \frac{1}{2}$	$0.97 \cdot \frac{1}{4} \cdot \frac{1}{2}$	$0.03 \cdot 0.63 \cdot \frac{1}{2}$	$0.03 \cdot 0.63 \cdot \frac{1}{6}$

electron):

$$\begin{aligned} \pi &\rightarrow \mu + \nu_\mu \\ K &\rightarrow \mu + \nu_\mu \\ \mu &\rightarrow e + \nu_\mu + \nu_e. \end{aligned} \quad (18)$$

It is important to include the kaon contribution. In fact, even though the branching ratio to produce kaons is ~ 30 times less than that for pion, since their maximum energy is often much higher, they dominate at high energies (Ando & Beacom 2005; Asano & Nagataki 2006).

Each intermediate particle also experiences cooling in a similar fashion to protons. The total cooling time for each of these is the same as for protons after changing $m_p \rightarrow m_i$, $i = \pi, K, \mu$, and there is no contribution from the Bethe-Heitler process or $p\gamma$. In addition, while muons do undergo hadronic cooling, the process is negligible (Bulmahn 2010). The fractional energy loss for hadronic interactions for pions and kaons is $\Delta E'_{\pi(K)}/E'_{\pi(K)} = 0.8$, the same as for pp interactions.

The final cooled spectra for neutrinos coming from the decay of the intermediates are modified in a similar way to the proton spectrum with a factor of $\eta^{-1} = \eta_\mu^{-1} + \eta_{\pi(K)}^{-1} + \eta_p^{-1}$, where the number of energy losses due to the intermediates is $\eta_i = t'_{i,c} m_i / E'_i \tau_i$ and τ_i is the rest frame lifetime of the particle. The proton parameters are calculated at the proton energy that corresponds to the given neutrino energy, related by a_i . The muon term is included only for neutrinos from a muon; for neutrinos directly from the mesons, no muon term is included. The multiplicity factors for these cooling processes are given in Table 1.

Figure 2 shows the cooling times for pions, muons, and kaons for GRB models with the same input parameters as for Fig. 1 as a function of the neutrino energy. For the adopted GRB parameters, the synchrotron cooling is the only process that affects the spectrum.

2.4. Input Energy Spectra for Protons and Photons

We assume that the central engine is accelerating protons to high energies (where the maximum energy is determined by the acceleration time and the cooling time, see Fig. 1 and Sec. 2.3.1). For protons, we assume an initial Fermi shock accelerated proton spectrum, $E_p'^{-2}$. This sets the initial power law for all subsequent spectra.

Photons are produced non-thermally inside a jet and are well described by a Band spectrum (Band et al. 1993),

$$\frac{dN_\gamma}{dE'_\gamma} \propto \begin{cases} \left(\frac{E'_\gamma}{E'_{\gamma,b}}\right)^{-1} \exp\left(-\frac{E'_\gamma}{E'_{\gamma,b}}\right) & E'_\gamma < E'_{\gamma,b} \\ \left(\frac{E'_\gamma}{E'_{\gamma,b}}\right)^{-2} \exp(-1) & E'_\gamma > E'_{\gamma,b} \end{cases}, \quad (19)$$

which is divergent as $E'_\gamma \rightarrow 0$. The photon spectrum is typ-

ically normalized over an experimentally motivated energy range, usually $E'_\gamma \in [1 \text{ keV}, 10 \text{ MeV}]$ applied in the jet frame and so that the total photon energy in that range is E'_{iso} . Note that in the case of optically thick sources, the photon distribution is expected to be thermal. However, in this case $\tau'_T > 1$ and therefore the jet cannot accelerate particles.

The photon break energy $E'_{\gamma,b}$ is given by the Amati relation (Amati et al. 2002):

$$\tilde{E}_{\gamma,b} = 0.364 \text{ MeV} \left(\frac{\tilde{E}_{\text{iso}}}{7.9 \times 10^{52} \text{ erg}} \right)^{0.51}. \quad (20)$$

Moreover, the Yonetoku relation relates the isotropic energy to the isotropic luminosity (Yonetoku et al. 2004),

$$\log_{10} \left(\frac{\tilde{E}_{\text{iso}}}{10^{52} \text{ erg}} \right) = 1.07 \log_{10} \left(\frac{\tilde{L}_{\text{iso}}}{10^{52} \text{ erg/s}} \right) + 0.66. \quad (21)$$

The isotropic energy is related to the jet energy by $\tilde{L}_{\text{iso}} = (4\pi \tilde{E}_j \epsilon_e) / (0.3 \tilde{r}_j \Omega_j)$, where the factor 0.3 is used as typically 0.3 times the peak luminosity represents the luminosity averaged over the burst duration (Kakuwa et al. 2012; Liu & Wang 2013). Although the above relations have been empirically derived and are based on observed GRBs, we will assume that these relations describe all jets.

2.5. Neutrino Energy Spectrum

For the neutrino spectrum, we take the proton spectrum $\propto E_p'^{-2}$ and multiply it by $\tau_{p\gamma}, \tau_{pp}$ for $p\gamma, pp$ interactions respectively. Since $\tau'_{pa} = \sigma_{pa} n'_a \tilde{r}_j / \Gamma$ (with $a = p, \gamma$), the effect of the photon break energy is automatically included by integrating over photon energies weighted by the photon spectrum. Then the unnormalized uncooled (unc) neutrino spectrum from initial pa interaction and intermediate $i \in \{\pi, \mu_\pi, K, \mu_K\}$ is,

$$\left. \frac{dN_\nu}{dE'_\nu} \right|_{i,\text{unc}} \propto E_\nu'^{-2} \left[\int dE'_\gamma \frac{dN_\gamma}{dE'_\gamma} \tau'_{p\gamma}(E'_p, E'_\gamma) + \tau'_{pp}(E'_p) \right], \quad (22)$$

where proton and neutrino energies are related by a_i (see Table 1) depending on which intermediate particle the neutrino comes from: $E'_p = E'_\nu / a_i$. The photon spectrum is normalized such that $\int dE'_\gamma \frac{dN_\gamma}{dE'_\gamma} = 1$.

We note that in the simple case where $\sigma_{p\gamma}$ is given by a step function at the Δ baryon threshold energy, we see that the $p\gamma$ correction to the $E_\nu'^{-2}$ part of the neutrino spectrum is $\propto E'_\nu$ before the first break and then $\propto \log E'_\nu$ after the first break until the spectrum cools to a softer spectrum after the second break. This is different than the conventionally used correction to $E_\nu'^{-2}$ which is $\propto E'_\nu, \propto 1, \propto E_\nu'^{-1}$. Our numerical results using the full $p\gamma$ cross section confirm this behavior shown in Fig. 3.

The total neutrino flux, accounting for the various energy loss mechanisms, is:

$$F_{\nu,i,a}(E_\nu) = \frac{(1+z)^3}{\Omega_j \Gamma d_L^2} N_a f_p \left[1 - \left(1 - \frac{\Delta E'_p}{E'_p} \right) \Big|_a^{\tau'_{pa}} \right] \left. \frac{dN_\nu}{dE'_\nu} \right|_{i,a}, \quad (23)$$

where $i = \pi, \mu_\pi, K, \mu_K$, $a = p, \gamma$, and the neutrino spectrum is normalized to the total jet energy, $\int dE'_\nu E'_\nu \frac{dN_\nu}{dE'_\nu} = E'_j$. The $[1 - (1 - \Delta E'_p / E'_p)^{\tau'_{pa}}]$ term accounts for the energy protons loss due to multiple $p\gamma$ and pp interactions. The remaining

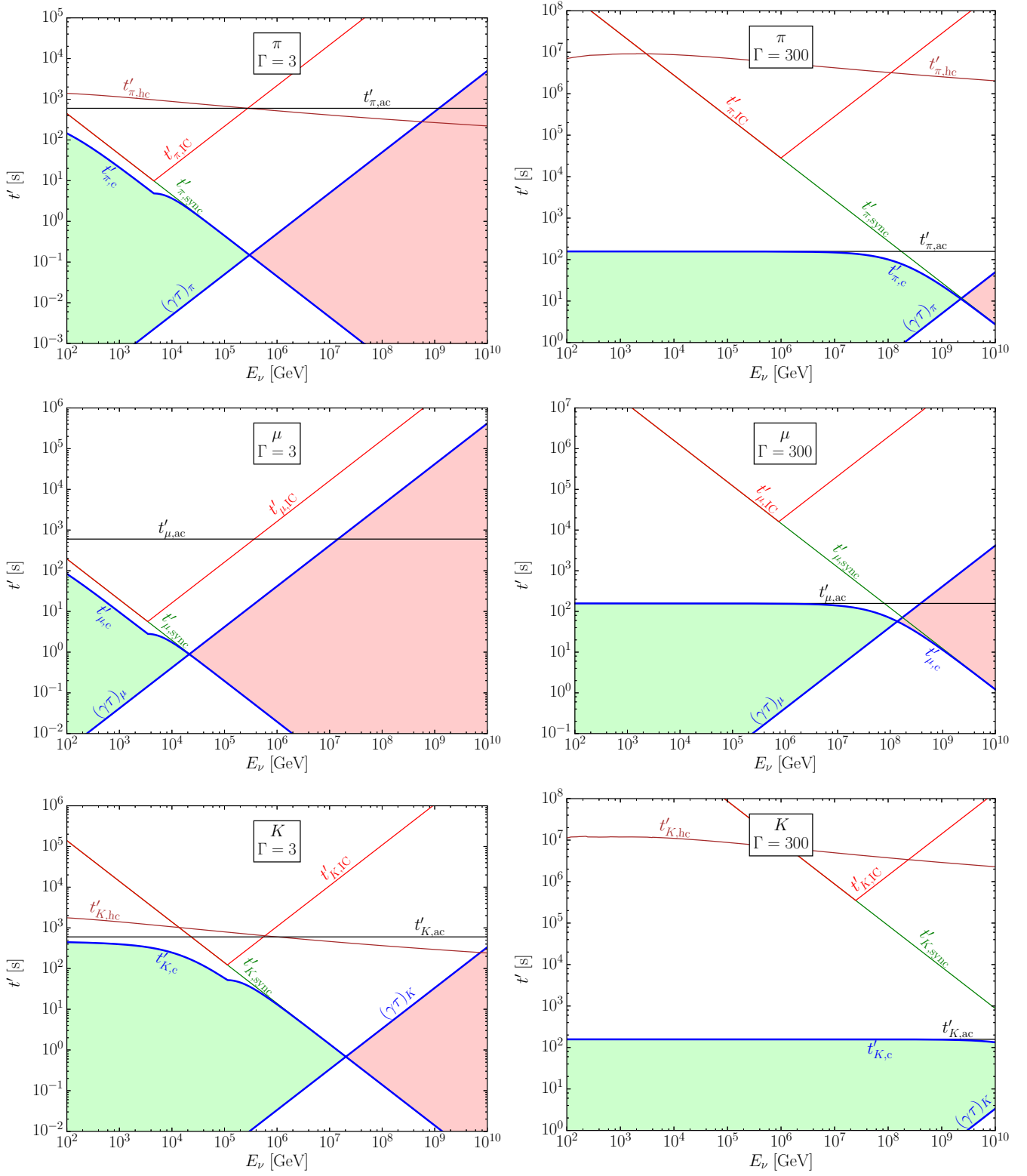


Figure 2. Cooling processes for pions (top), muons (middle), and kaons (bottom) as a function of the corresponding neutrino energy in the observer frame for $\Gamma = 3$ on the left and $\Gamma = 300$ on the right. The jet energy is fixed to $\bar{E}_j = 10^{51}$ erg, the energy fractions are $\epsilon_e = \epsilon_B = 0.1$, and the redshift is $z = 1$, the same as in Fig. 1. The thin solid lines are the various individual cooling processes; the tick lines are the total cooling, and the decay time. The green shaded region on the left of each figure shows the largely uncooled portion of the spectrum, while the red region on the right shows the cooled portion of the spectrum. For the adopted input parameters, synchrotron cooling is the only process that affects the spectrum.

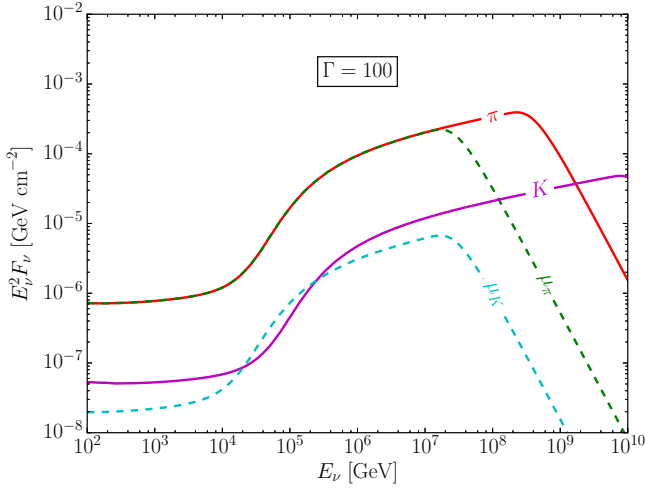


Figure 3. Neutrino fluence observed at Earth for the simple GRB model as a function of the observed E_ν from one GRB with $\Gamma = 100$, jet energy $\tilde{E}_j = 10^{51}$ erg, energy fractions $\epsilon_e = \epsilon_B = 0.1$, and redshift $z = 1$, broken up into the different contributions coming from the intermediate particles. The pp contribution is the nearly flat part at low energies, while the $p\gamma$ component is rising at lower energies. The latter experiences the characteristic break at an energy related to the photon break energy. The cutoff energy is given by cooling and decay timescales. The μ_π curve lays exactly on top of the π curve at lower energies, a result of the fact that $a_\pi = a_{\mu_\pi}$.

term accounts for energy loss from intermediate cooling, and is

$$f_p = \frac{\int dE'_\nu E'_\nu \left. \frac{dN_\nu}{dE'_\nu} \right|_{c,pp+p\gamma}}{\int dE'_\nu E'_\nu \left. \frac{dN_\nu}{dE'_\nu} \right|_{pc,pp+p\gamma}}, \quad (24)$$

where pc in the denominator refers to the fact that we include only proton cooling and not the cooling of secondaries in that integral.

Figure 3 shows the neutrino fluence observed at Earth from one source for $\Gamma = 100$, jet energy $\tilde{E}_j = 10^{51}$ erg, energy fractions $\epsilon_e = \epsilon_B = 0.1$, and redshift $z = 1$ for each of the four intermediates. The contribution due to pp interactions is mostly visible at low energies (the flat tail of the spectrum), while the $p\gamma$ component is rising at lower energies and then experiences the various cooling processes described above.

The per-flavor neutrino flux before flavor oscillations is,

$$\begin{aligned} F_{\nu_e, \text{unosc}} &= F_{\nu_e, \mu_\pi} + F_{\nu_e, \mu_K} \\ F_{\nu_\mu, \text{unosc}} &= F_{\nu_\mu, \pi} + F_{\nu_\mu, \mu_\pi} + F_{\nu_\mu, K} + F_{\nu_\mu, \mu_K}. \end{aligned} \quad (25)$$

Neutrinos oscillate en route to Earth and the distance averaged oscillated flux is (Anchordoqui et al. 2014b):

$$\begin{aligned} F_{\nu_\mu, \text{osc}} &= \frac{1}{4} \sin^2 2\theta_{12} F_{\nu_e, \text{unosc}} \\ &\quad + \frac{1}{8} (4 - \sin^2 2\theta_{12}) F_{\nu_\mu, \text{unosc}}, \end{aligned} \quad (26)$$

$$\begin{aligned} F_{\nu_e, \text{osc}} &= \left(1 - \frac{1}{2} \sin^2 2\theta_{12}\right) F_{\nu_e, \text{unosc}} \\ &\quad + \frac{1}{4} \sin^2 2\theta_{12} F_{\nu_\mu, \text{unosc}}, \end{aligned} \quad (27)$$

with $\theta_{12} = 33.5^\circ$ (Esteban et al. 2017). While neutrino oscillations through the stellar envelope do result in matter effects for $E_\nu \lesssim 10$ TeV (Mena et al. 2007; Sahu & Zhang 2010;

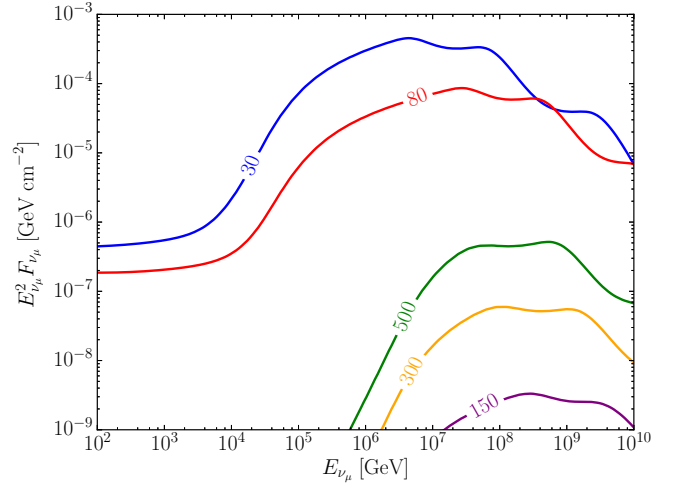


Figure 4. Oscillated ν_μ fluence for the simple GRB model as a function of the observed E_ν , as seen at Earth from one GRB for different values of Γ , jet energy $\tilde{E}_j = 10^{51}$ erg, energy fractions $\epsilon_e = \epsilon_B = 0.1$, and redshift $z = 1$. The contribution from pp interactions is subdominant compared to the $p\gamma$ one except at low energies.

Osorio Oliveros et al. 2013), in our analysis we will focus on neutrino energies larger than $\gtrsim 10$ TeV as those are better constrained by the IceCube data; hence neutrino oscillations in the source are neglected in this work.

Figure 4 shows the oscillated muon neutrino fluence from one source for jet energy $\tilde{E}_j = 10^{50}$ erg, energy fractions $\epsilon_e = \epsilon_B = 0.1$, and redshift $z = 1$ as a function of the neutrino energy for different values of Γ . As expected the pp contribution, the nearly flat part at low energies, is subdominant compared to the $p\gamma$ contribution except at energies where IceCube's sensitivity to astrophysical neutrinos is low due to large atmospheric backgrounds. Moreover, we have restricted ourselves to the high energy starting event (HESE) data set which contains neutrinos with $E_\nu \gtrsim 40$ TeV and has very low backgrounds.

3. NEUTRINO DIFFUSE EMISSION IN THE SIMPLE GRB MODEL

The first model we will consider is the simple GRB model where every jet has one Lorentz boost factor Γ for the entire jet. The population of jets will be sampled from a distribution of Γ 's that describe the data well.

To calculate the diffuse neutrino intensity from GRBs, we assume that the GRB rate, $R(z, \Gamma) dz d\Gamma$, is separable into $R(z, \Gamma) dz d\Gamma = R(z) \xi(\Gamma) dz d\Gamma$ with,

$$R(z) \propto \left[(1+z)^{p_1 k} + \left(\frac{1+z}{5000} \right)^{p_2 k} + \left(\frac{1+z}{9} \right)^{p_3 k} \right]^{1/k}, \quad (28)$$

where $k = -10$, $p_1 = 3.4$, $p_2 = -0.3$, $p_3 = -3.5$ are the fit parameters to the star formation rate from (Yuksel et al. 2008). In fact, we assume that the CCSN rate (and in turn the rate of choked and bright GRBs) follows the star-formation rate (Horiuchi et al. 2013; Dahlen et al. 2012). This function $R(z)$ is composed of three parts with power laws p_1 , p_2 , and p_3 with breaks at $z_1 \approx 1$ and $z_2 \approx 4$, and is normalized to $R(0) = 1$.

We make the ansatz that $\xi(\Gamma)$ follows a power law² $\xi(\Gamma) = \beta \Gamma^{\alpha}$ (Tamborra & Ando 2016). We then constrain the power law by the measured HL-GRB rate for jets with $\Gamma > 200$, and

² Note that a linear function does not in general remain non-zero when fit to the given criteria. Hence, we only use the power law parameterization.

the known CCSN rate for all jets:

$$R_{\text{SN}}(0)\zeta_{\text{SN}}\frac{\langle\Omega_j\rangle}{4\pi} = \int_1^{1000} d\Gamma \xi(\Gamma), \quad (29)$$

$$\rho_{0,\text{HL-GRB}} = \int_{200}^{1000} d\Gamma \xi(\Gamma), \quad (30)$$

where $R_{\text{SN}}(0) \approx 2 \times 10^5 \text{ Gpc}^{-3} \text{ yr}^{-1}$ (Dahlen et al. 2004; Strolger et al. 2015) is the local CCSN rate, $\zeta_{\text{SN}} \in (0, 1]$ is the fraction of CCSNe that form jets and is taken to be redshift independent. The rate $\rho_{0,\text{HL-GRB}} \approx 0.8 \text{ Gpc}^{-3} \text{ yr}^{-1}$ is an optimistic estimation for the observed local HL-GRB rate (Wanderman & Piran 2010). We use the range $\Gamma \in [200, 1000]$ to define HL-GRB's motivated by *Fermi-LAT* (Ackermann et al. 2011). The mean fraction of jets pointing toward the Earth $\langle\Omega_j\rangle/4\pi$ is

$$\langle\Omega_j\rangle = \frac{\int_1^{1000} d\Gamma \xi(\Gamma)\Omega_j}{\int_1^{1000} d\Gamma \xi(\Gamma)}, \quad (31)$$

since Ω_j is a function of Γ . For example, for our canonical GRB model with $\zeta_{\text{SN}} = 0.1$, we get $\alpha_\Gamma = -2.6$ and $\beta_\Gamma = 6.7 \times 10^3 \text{ Gpc}^{-3} \text{ yr}^{-1}$.

The resultant diffuse neutrino intensity from GRBs is,

$$I_\nu(E_\nu) = \int_1^{1000} d\Gamma \int_{z_{\min}}^{z_{\max}} dz \frac{cd_L^2(1+z)^{-3}}{H_0 E(z)} R(z, \Gamma) F_\nu(E_\nu), \quad (32)$$

with $d_L(z)$ the luminosity distance, $E(z) = \sqrt{\Omega_M(1+z)^3 + \Omega_\Lambda}$ (Hogg 1999) computed by taking $\Omega_M = 0.31$, $\Omega_\Lambda = 0.69$, $H_0 = 68 \text{ km/s/Mpc}$ (Ade et al. 2016), and $[z_{\min}, z_{\max}] = [0, 10]$. We require $\theta_j < \pi/2$ in Eq. 32; if the jet would be larger than that we set the flux to zero.

The resultant diffuse neutrino intensity is plotted in the top panel of Fig. 5 for different values of ζ_{SN} along with the six year HESE data from IceCube (Aartsen et al. 2015d). Noticeably, according to \tilde{E}_j and ζ_{SN} , only a small fraction of all CCSNe gives origin to a successful jet, as shown in Fig. 6.

4. NEUTRINO DIFFUSE EMISSION IN THE ADVANCED GRB MODEL

In this Section, we take a somewhat more realistic model of the physics within a jet and allow for Γ to vary across the jet angle from some maximum value Γ_{\max} at the center of the jet ($\theta = 0$) out to $\Gamma = 1$: the advanced GRB model. In this model, we do not rely on $\theta_j = 1/\Gamma$ anymore. Since we anticipate that multiple shocks will be accelerating the protons, the resulting Γ distribution is a von-Mises-Fisher distribution,

$$\Gamma(\theta) = \Gamma_{\max} \exp[\kappa(\cos\theta - 1)], \quad (33)$$

where the concentration $\kappa \approx 1/\sigma^2$ for σ small, with σ the usual standard deviation. We take $\sigma = 1/\sqrt{\Gamma_{\max}}$ motivated by random walks of the accelerated particles within the jet. In this model we define the volume of the jet (Eq. 3) with $\theta_j \rightarrow \theta_{\max}$ where θ_{\max} is defined by $\Gamma(\theta_{\max}) = 1$, or

$$\theta_{\max} = \cos^{-1}\left(1 - \frac{\ln \Gamma_{\max}}{\kappa}\right). \quad (34)$$

We note that for $\kappa = \Gamma_{\max}$, θ_{\max} has a maximum at $\Gamma_{\max} = e$. For a representative jet with $\Gamma_{\max} = 300$ this corresponds to $\theta_{\max} = 11^\circ$.

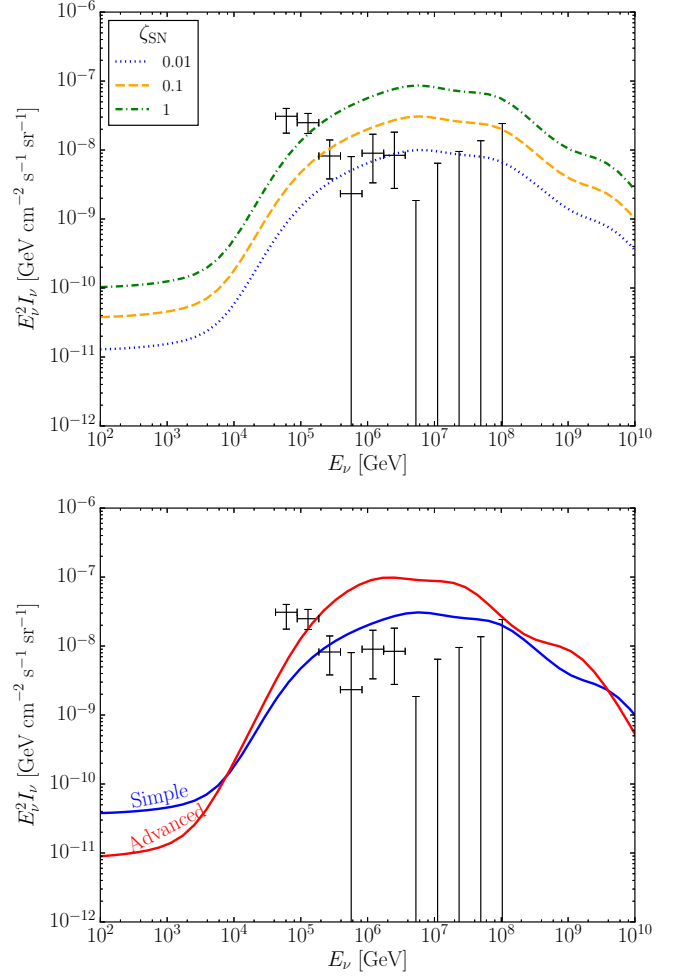


Figure 5. Diffuse neutrino intensities for GRBs with jet energy $\tilde{E}_j = 10^{51}$ erg, energy fractions $\epsilon_e = \epsilon_B = 0.1$ plotted against the six year HESE data from IceCube (Aartsen et al. 2015d). Top panel: Diffuse neutrino intensity from the simple GRB model obtained for different values of ζ_{SN} ($\zeta_{\text{SN}} = 0.01$ in dotted blue, 0.1 in dashed orange and 1 for the dash-dotted green curve). The expected diffuse intensity is larger for larger values of ζ_{SN} . Bottom panel: Diffuse neutrino intensity obtained for the simple and advanced GRB model with $\zeta_{\text{SN}} = 0.1$. The overall diffuse intensity is comparable within both models.

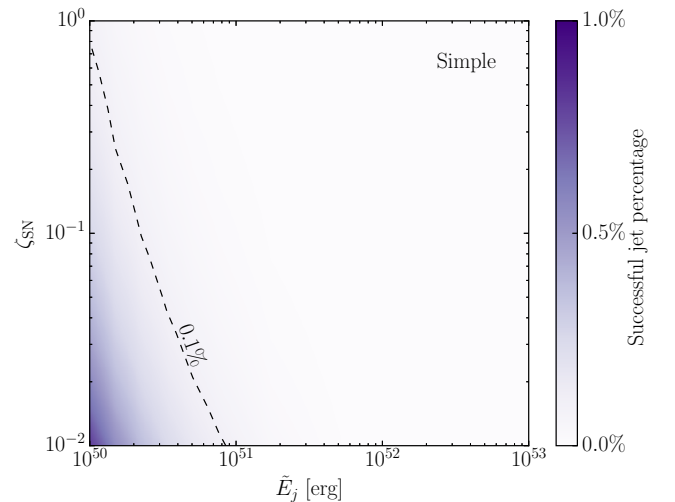


Figure 6. Fraction of successful jets in the $(\tilde{E}_j, \zeta_{\text{SN}})$ plane for the simple GRB model. Only a small fraction of all CCSNe can harbor a successful jet.

The component of the GRB rate $R(z, \Gamma)$ introduced in Sec. 3 depending on Γ is assumed to follow a distribution similarly defined as in the previous section but this time this is a function of Γ_{\max} : $\xi(\Gamma_{\max}) = \beta_{\Gamma} \Gamma_{\max}^{\alpha_{\Gamma}}$.

The constraint in Eq. 30 to reproduce the observed HL-GRB rate becomes,

$$\rho_{0, \text{HL-GRB}} = \int_{200}^{1000} d\Gamma_{\max} \int_{\Omega(\theta < \theta_{\max})} \frac{d\Omega}{4\pi} \xi(\Gamma_{\max}). \quad (35)$$

The maximum value of $\cos \theta$ is 1 and the minimum value of $\cos \theta$ (the maximum value of θ) is when $\Gamma = 200$, which is $\cos \theta_{\min} = 1 - \ln(\Gamma_{\max}/200)/\kappa$.

$$\rho_{0, \text{HL-GRB}} = \frac{\beta_{\Gamma}}{\alpha_{\Gamma}^2} \left[(200^{\alpha_{\Gamma}} - 1000^{\alpha_{\Gamma}}) + \alpha_{\Gamma} 1000^{\alpha_{\Gamma}} \ln \frac{1000}{200} \right]. \quad (36)$$

Similarly to Eq. 29, for the advanced GRB model we have

$$\begin{aligned} R_{\text{SN}}(0) \zeta_{\text{SN}} &= \int_1^{1000} d\Gamma_{\max} \xi(\Gamma_{\max}) \\ &= \frac{\beta_{\Gamma}}{\alpha_{\Gamma} + 1} (1000^{\alpha_{\Gamma} + 1} - 1), \end{aligned} \quad (37)$$

where the beaming angle factor on each side has canceled.

The diffuse neutrino intensity is

$$\begin{aligned} I_{\nu}(E_{\nu}) &= \int_1^{1000} d\Gamma_{\max} \int_{\cos \theta_{\max}}^1 d(\cos \theta) \int_{z_{\min}}^{z_{\max}} dz \\ &\quad \times \frac{cd_L^2(1+z)^{-3}}{H_0 E(z)} R(z, \Gamma_{\max}) F_{\nu}(E_{\nu}). \end{aligned} \quad (38)$$

The $\cos \theta$ integral goes over $\theta \in [0, \theta_{\max}]$, and we again require that the jet can successfully accelerate protons.

The fraction of successful jets for this model is shown in the top panel of Fig. 7. One can see that the fraction of CCSNe harboring successful jets is larger in this model with respect to the simple GRB model, given the different scaling laws intrinsic to the models.

The total diffuse neutrino intensity for our canonical GRB and $\zeta_{\text{SN}} = 0.1$ for all successful jets is plotted in the bottom panel of Fig. 5 for the advanced GRB model to be compared with the one from the simple GRB model. Both models produce comparable intensities.

We now turn to the issue of electromagnetically choked jets. Depending on the jet properties, we expect that there will be some successful jets that are choked or invisible. In the simple model, all of the jets are bright if they successfully form. On the other hand, among all successful jets, the fraction of choked jets for the advanced model is shown in the bottom panel of Fig. 7. Below $\tilde{E}_j \sim 5 \times 10^{51}$ erg, we find that 50% of the jets are choked; while below $\tilde{E}_j \sim 2 \times 10^{51}$ erg, we obtain that 90% of the jets are choked. Note that, for the usually assumed typical GRB jet energy ($\tilde{E}_j \sim 3 \times 10^{51}$ erg), we expect that $\sim 70\%$ of the jets are choked.

5. ICECUBE CONSTRAINTS ON THE CCSN-GRB CONNECTION

We then construct a χ^2 test with the IceCube data where we allow for neutrinos from jetted bursts to contribute a subdominant component of the observed astrophysical flux,

$$\chi^2 = \sum_i \left[\frac{I(E_i) - I_{\text{IC}}(E_i)}{I_{\text{IC}, +1\sigma}(E_i) - I_{\text{IC}}(E_i)} \right]^2 \Theta [I(E_i) - I_{\text{IC}}(E_i)], \quad (39)$$

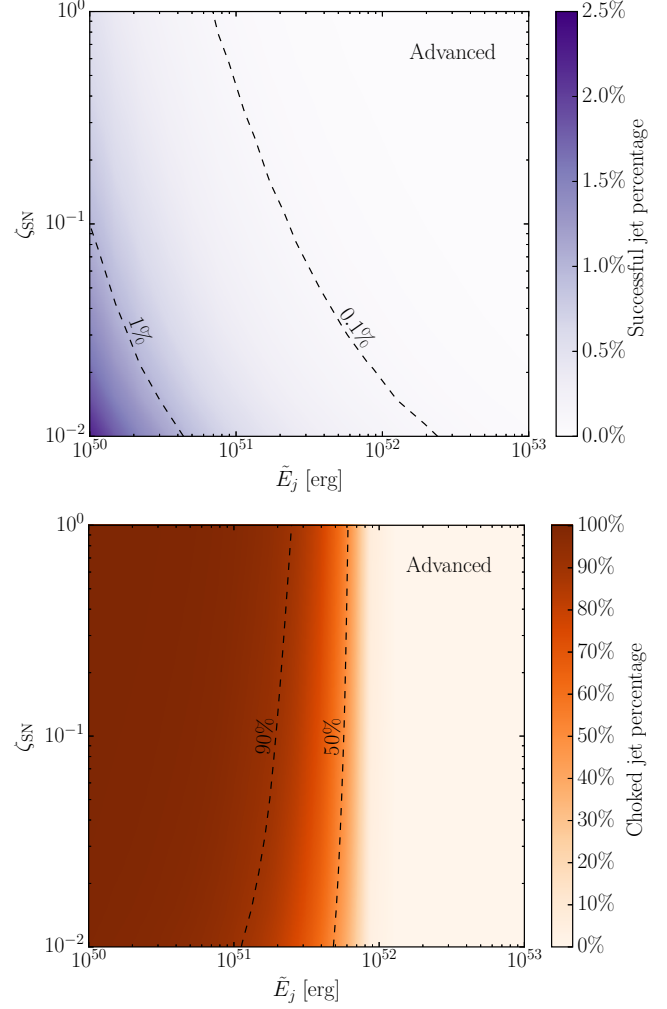


Figure 7. Top panel: Fraction of successful jets in the $(\tilde{E}_j, \zeta_{\text{SN}})$ plane for the advanced GRB model. Bottom panel: Fraction of jets that are choked for the advanced GRB model. Below $\tilde{E}_j \sim 5 \times 10^{51}$ erg, 50% of the jets are choked; below $\tilde{E}_j \sim 2 \times 10^{51}$ erg, 90% of the jets are choked.

where the sum is over nine energy bins in the range [40 TeV, 20 PeV] which includes four bins with zero events.

We do not include two of the energy bins in the χ^2 that are likely under-fluctuations: the “dip” and the “Glashow” bins centered at $E_{\nu} = 570$ TeV and 5.3 PeV respectively. These bins have been investigated in the literature as possible evidence of new physics (Anchordoqui et al. 2014a; Learned & Weiler 2014; DiFranzo & Hooper 2015; Tomar et al. 2015). Under the assumption of no new physics, these bins are almost certainly under-fluctuations and unduly push up the χ^2 . Moreover, IceCube has seen a through going track event with deposited energy of 2.6 PeV (Schoenen & Raedel 2015), which corresponds to a higher neutrino energy of $\sim 5 - 10$ PeV. This would suggest that the zero bins in the data will in fact be filled in with future data. Finally, the “dip” bin has already begun to be filled in since the initial deficit also suggesting that it is an under-fluctuation from the first few years of data.

We then scan jet energies (\tilde{E}_j) and the fraction of CCSN that form jets (ζ_{SN}) and determine the significance of the resulting intensity given the data. Figure 8 shows the 90% contour levels for both the simple and advanced GRB models. We note that the simple GRB model starts becoming increasingly con-

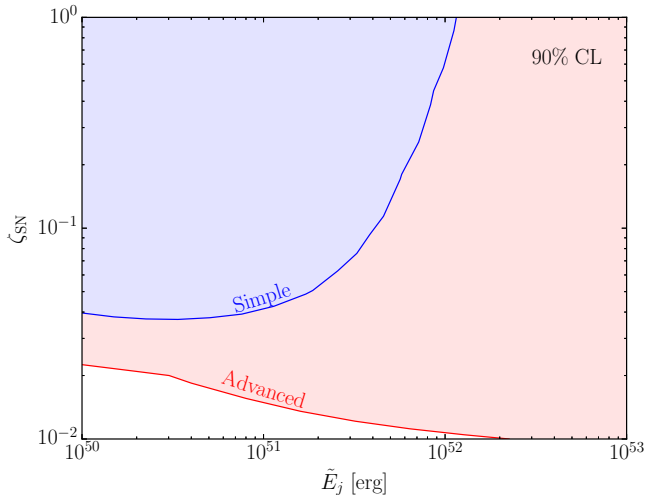


Figure 8. Contour plot of the fraction of allowed bursts in the $(\tilde{E}_j, \zeta_{\text{SN}})$ plane for the simple and the advanced GRB model. The shaded regions are excluded by the IceCube data (Aartsen et al. 2015c) at 90% CL (7 dof). The two models lead to comparable results for $\tilde{E}_j \lesssim 3 \times 10^{51}$ erg, while they differ for larger \tilde{E}_j since most of the jets are unsuccessful at accelerating protons within the simple GRB model. For a typical jet energy $\tilde{E}_j \approx 3 \times 10^{51}$ erg, about 1% of all CCSNe can harbor jets.

sistent with the IceCube data above $\tilde{E}_j \sim 10^{51}$ erg due to an increasing fraction of the jets becoming unsuccessful at accelerating protons. On the other hand, the two GRB models give comparable results for $\tilde{E}_j \lesssim 3 \times 10^{51}$ erg. Our findings are discussed in the next section.

6. DISCUSSION

For a typical jet energy $\tilde{E}_j \approx 3 \times 10^{51}$ erg, Figs. 7 and 8 suggest that less than 1% of all CCSNe can harbor jets. Most of those jets are predicted to be choked. This fraction should be compared with existing empirical constraints, based on electromagnetic observations of bright jets, suggesting that most likely a subsample of CCSNe could further evolve in jets (Guetta & Della Valle 2007; Grieco et al. 2012; Modjaz et al. 2014; Margutti et al. 2014; Sobacchi et al. 2017).

It has been estimated that, under the assumption that all SN Ib/c harbor a jet, less than 10% of these manages to break out from the stellar envelope and further power a prompt emission visible in γ 's (Sobacchi et al. 2017; Soderberg et al. 2004, 2006). Similarly, Grieco et al. (2012) finds that the ratio of GRB to type Ib/c SNe is about 0.1 – 1% in the local universe where type Ib/c SNe comprise up to $\sim 10\%$ of all SNe. The smaller sub-class of broadlined SNe has been linked to GRBs even in the absence of observed gamma-ray emission (Podsiadlowski et al. 2004; Mazzali et al. 2005; Soderberg et al. 2006; Soderberg 2006; Milisavljevic et al. 2015; Milisavljevic & Fesen 2017). Interestingly, our findings are compatible with the above observational constraints and suggest that the large majority of jets harbored in CCSNe should be not electromagnetically visible. Additionally, Fesen & Milisavljevic (2016) finds evidence that Cassiopeia A, categorized as a type Ib, may have had a weak jet, which could have either been unsuccessful at accelerating particles or choked and further suggests that all jets may be a part of a single continuous distribution.

Given the uncertainties on the CCSN explosion mechanism

and concerning the conditions leading to the jet formation, we refrain from establishing a firm connection to a specific CCSN subclass in our model and instead rely on the whole CCSN population. Nevertheless, our model, being very general, does automatically take into account any eventual relativistic supernovae (Soderberg et al. 2010; Soderberg et al. 2006; Chakraborti et al. 2015) not directly linked to an electromagnetically bright GRB as a subclass of all stellar explosions possibly harboring jets (Margutti et al. 2014; Lazzati et al. 2012).

It is worth noticing that our estimation does not take into account any dependence of the CCSN–GRB rate as a function of the redshift and progenitor metallicity (Grieco et al. 2012; Levesque et al. 2010; Perley et al. 2013). Moreover, there may be additional metallicity/redshift dependence for the choked jets that does not apply to the electromagnetically bright GRBs.

Our findings depend on the assumption of maximally efficient particle acceleration in the jet. The fraction of the jet energy accelerating particles and further leading to the production of neutrinos and photons is currently unconstrained; this should enter as a constant normalization factor in the estimation of the diffuse neutrino intensity. However, if particle acceleration should not be fully efficient in the jet then one should expect a correspondingly weaker upper bound on ζ_{SN} . The scan of different possible values of \tilde{E}_j should anyway give an idea of the range of ζ_{SN} compatible with the data even in the case of less efficient particle acceleration.

7. CONCLUSIONS

Jets harbored in core-collapse supernovae (CCSNe) are promising sources of high energy neutrinos. By relying on the collapsar model, we assume that similar physical processes govern both electromagnetically bright and “choked” gamma-ray bursts (GRBs). Our calculations include neutrino production from both $p\gamma$ and pp interactions and account for cooling effects of protons, pions, kaons, and muons.

Three relevant classes of jets are investigated. These classes are based on whether or not a jet successfully accelerates protons and whether or not the jet escapes the stellar envelope. If the jet is optically thick, then it is unsuccessful and no high energy photons or neutrinos are produced. Successful jets can then be either visible, if photons escape the stellar envelope, or choked if the jet does not escape. In either of these two cases, high energy neutrinos are produced.

We calculate the neutrino diffuse intensity for two different scaling relations between the opening angle θ_j and the Lorentz boost factor Γ . The “simple” GRB model assumes the classical $\theta_j = 1/\Gamma$ relation, with Γ considered to be the same throughout the jet. On the other hand, the “advanced” GRB model takes a Γ distribution throughout the jet. Γ is assumed to be highest along the jet axis and decrease down to one on the edges of the jet, similarly to what should occur in a more realistic case. In the advanced GRB case, the characteristic width of the jet is given by $1/\sqrt{\Gamma_{\text{max}}}$ where Γ_{max} is the Lorentz boost factor at $\theta = 0$. Our model is then tuned on the observed rate of high-luminosity GRBs and the CCSN rate. We adopt the flux of high-energy neutrinos measured by IceCube as an upper limit to the possible neutrino flux coming from bright and choked GRBs.

We find that while all of the jets in the simple GRB model are electromagnetically bright, the majority of the jets in the advanced GRB model are choked for jet energies $\tilde{E}_j \lesssim 5 \times 10^{51}$ erg, given the differences in the scaling laws of the two GRB

models. This implies that it is crucial to adopt a refined modeling of the GRB microphysics in order to constraint the jet properties. In fact, for both models, the compatibility with the IceCube data (Aartsen et al. 2017b) is similar for $\dot{E}_j \lesssim 10^{51}$ erg with the advanced model being slightly more constrained. Starting above $\dot{E}_j \sim 10^{51}$ erg, an increasing number of jets in the simple GRB model is unsuccessful leading to a smaller diffuse intensity.

Noticeably, our findings suggest that at most 1% of all CCSNe can harbor jets. Interestingly, those jets are mostly choked. This fraction is competitive with existing empirical and observational constraints suggesting that an even smaller fraction can further lead to electromagnetically bright GRBs.

Our study constitutes a step forward towards a realistic and general modeling of the neutrino production within bright and choked jets. It still relies on several simplifying assumptions however, e.g. it does not take into account any feature due to the metallicity and progenitor dependence of the CCSN population and only considers acceleration at the internal-shock radius. As a consequence, our bounds should provide results in the correct ballpark, but may still suffer changes within a more sophisticated population-dependent modeling.

This work proves that neutrinos could be powerful messengers of the burst physics. In the light of the increasing IceCube statistics, neutrinos could provide major insights on the CCSN–GRB connection in the next future.

We are grateful to Jochen Greiner, Jens Hjorth, and Hans-Thomas Janka for useful discussions. PBD and IT acknowledge support from the Villum Foundation (Project No. 13164), and the Danish National Research Foundation (DNRF91). PBD thanks the Danish National Research Foundation (Grant No. 1041811001) for support during the final stages of this project. The work of IT has also been supported by the Knud Højgaard Foundation and the Deutsche Forschungsgemeinschaft through Sonderforschungsbereich SFB 1258 “Neutrinos and Dark Matter in Astro- and Particle Physics (NDM).

REFERENCES

- Aartsen, M. G. et al. 2013a, *Science*, 342, 1242856
 —. 2013b, *Phys. Rev. Lett.*, 111, 021103
 —. 2014, *Phys. Rev. Lett.*, 113, 101101
 —. 2015a, *Astrophys. J.*, 809, 98
 —. 2015b, *Phys. Rev.*, D91, 022001
 —. 2015c, *Phys. Rev. Lett.*, 115, 081102
 Aartsen, M. G. et al. 2015d, in *Proceedings, 34th International Cosmic Ray Conference (ICRC 2015): The Hague, The Netherlands, July 30-August 6, 2015*
 —. 2017a, arXiv:1707.03416 [astro-ph.HE]
 —. 2017b, *Astrophys. J.*, 843, 112
 Ackermann, M. et al. 2011, *Astrophys. J.*, 729, 114
 Ade, P. A. R. et al. 2016, *Astron. Astrophys.*, 594, A13
 Amati, L. et al. 2002, *Astron. Astrophys.*, 390, 81
 Anchoordoqui, L. A., Barger, V., Goldberg, H., Learned, J. G., Marfatia, D., Pakvasa, S., Paul, T. C., & Weiler, T. J. 2014a, *Phys. Lett.*, B739, 99
 Anchoordoqui, L. A. et al. 2014b, *JHEAp*, 1-2, 1
 Ando, S. & Beacom, J. F. 2005, *Phys. Rev. Lett.*, 95, 061103
 Asano, K. & Nagataki, S. 2006, *Astrophys. J.*, 640, L9
 Baerwald, P., Hummer, S., & Winter, W. 2012, *Astropart. Phys.*, 35, 508
 Band, D. et al. 1993, *Astrophys. J.*, 413, 281
 Bartos, I., Beloborodov, A. M., Hurley, K., & Márka, S. 2013, *Phys. Rev. Lett.*, 110, 241101
 Bromberg, O., Nakar, E., & Piran, T. 2011a, *Astrophys. J.*, 739, L55
 Bromberg, O., Nakar, E., Piran, T., & Sari, R. 2011b, *Astrophys. J.*, 740, 100
 Bulmahn, A. P. 2010, PhD thesis, Iowa U.
 Campana, S. et al. 2006, *Nature*, 442, 1008
 Cenko, S. B. et al. 2011, *Astrophys. J.*, 732, 29
 Chakraborti, S. et al. 2015, *Astrophys. J.*, 805, 187
 Dahlen, T., Strolger, L.-G., Riess, A. G., Mattila, S., Kankare, E., & Mobasher, B. 2012, *Astrophys. J.*, 757, 70
 Dahlen, T. et al. 2004, *Astrophys. J.*, 613, 189
 Daigne, F. & Mochkovitch, R. 2007, *Astron. Astrophys.*, 465, 1
 Denton, P. B., Marfatia, D., & Weiler, T. J. 2017, *JCAP*, 1708, 033
 Dermer, C. D., Murase, K., & Inoue, Y. 2014, *JHEAp*, 3-4, 29
 DiFranzo, A. & Hooper, D. 2015, *Phys. Rev.*, D92, 095007
 Esteban, I., Gonzalez-García, M. C., Maltoni, M., Martínez-Soler, I., & Schwetz, T. 2017, *JHEP*, 01, 087
 Fesen, R. A. & Milisavljevic, D. 2016, *Astrophys. J.*, 818, 17
 Gehrels, N. & Razzaque, S. 2013, *Front. Phys.(Beijing)*, 8, 661
 Goldstein, A., Connaughton, V., Briggs, M. S., & Burns, E. 2016, *Astrophys. J.*, 818, 18
 Grieco, V., Matteucci, F., Meynet, G., Longo, F., Della Valle, M., & Salvaterra, R. 2012, *Monthly Notices of the Royal Astronomical Society*, 423, 3049
 Guetta, D. & Della Valle, M. 2007, *Astrophys. J.*, 657, L73
 Gupta, N. & Zhang, B. 2007, *Astropart. Phys.*, 27, 386
 He, H.-N., Liu, R.-Y., Wang, X.-Y., Nagataki, S., Murase, K., & Dai, Z.-G. 2012, *Astrophys. J.*, 752, 29
 Hjorth, J. 2013, *Phil. Trans. Roy. Soc. Lond.*, A371, 20120275
 Hjorth, J. & Bloom, J. S. 2012, *CAPS*, 51, 169
 Hogg, D. W. 1999, arXiv:astro-ph/9905116
 Horiuchi, S. & Ando, S. 2008, *Phys. Rev.*, D77, 063007
 Horiuchi, S., Beacom, J. F., Bothwell, M. S., & Thompson, T. A. 2013, *Astrophys. J.*, 769, 113
 Kakuwa, J., Murase, K., Toma, K., Inoue, S., Yamazaki, R., & Ioka, K. 2012, *Mon. Not. Roy. Astron. Soc.*, 425, 514
 Kumar, P. & Zhang, B. 2014, *Phys. Rept.*, 561, 1
 Lazzati, D., Morsony, B. J., Blackwell, C. H., & Begelman, M. C. 2012, *Astrophys. J.*, 750, 68
 Learned, J. G. & Weiler, T. J. 2014, arXiv:1407.0739 [astro-ph.HE]
 Levesque, E. M. et al. 2010, *Astrophys. J.*, 709, L26
 Liang, E., Zhang, B., & Dai, Z. G. 2007, *Astrophys. J.*, 662, 1111
 Liu, R.-Y. & Wang, X.-Y. 2013, *Astrophys. J.*, 766, 73
 Liu, R.-Y., Wang, X.-Y., & Dai, Z.-G. 2011, *Mon. Not. Roy. Astron. Soc.*, 418, 1382
 Lü, H., Wang, X., Lu, R., Lan, L., Gao, H., Liang, E., Graham, M. L., Zheng, W., Filippenko, A. V., & Zhang, B. 2017, *Astrophys. J.*, 843, 114
 MacFadyen, A. & Woosley, S. E. 1999, *Astrophys. J.*, 524, 262
 MacFadyen, A. I., Woosley, S. E., & Heger, A. 2001, *Astrophys. J.*, 550, 410
 Margutti, R. et al. 2014, *Astrophys. J.*, 797, 107
 Mazzali, P. A. et al. 2005, *Science*, 308, 1284
 Mena, O., Mocioiu, I., & Razzaque, S. 2007, *Phys. Rev.*, D75, 063003
 Milisavljevic, D. & Fesen, R. A. 2017
 Milisavljevic, D. et al. 2015, *Astrophys. J.*, 799, 51
 Modjaz, M. 2011, *Astron. J.*, 332, 434
 Modjaz, M. et al. 2014, *Astron. J.*, 147, 99
 Murase, K., Guetta, D., & Ahlers, M. 2016, *Phys. Rev. Lett.*, 116, 071101
 Murase, K. & Ioka, K. 2013, *Phys. Rev. Lett.*, 111, 121102
 Murase, K., Ioka, K., Nagataki, S., & Nakamura, T. 2006, *Astrophys. J.*, 651, L5
 Mészáros, P. 2006, *Rept. Prog. Phys.*, 69, 2259
 —. 2017, in *Neutrino Astronomy- Current status, future prospects (World Scientific)*, 1–14, arXiv:1511.01396 [astro-ph.HE]
 Mészáros, P. & Waxman, E. 2001, *Phys. Rev. Lett.*, 87, 171102
 Nakar, E. 2015, *Astrophys. J.*, 807, 172
 Osorio Oliveros, F. A., Sahu, S., & Sanabria, J. C. 2013, *Eur. Phys. J.*, C73, 2574
 Paczynski, B. 1998, *Astrophys. J.*, 494, L45
 Palladino, A. & Vissani, F. 2016, *Astrophys. J.*, 826, 185
 Patrignani, C. et al. 2016, *Chin. Phys.*, C40, 100001
 Perley, D. A. et al. 2013, *Astrophys. J.*, 778, 128
 Podsiadlowski, P., Mazzali, P. A., Nomoto, K., Lazzati, D., & Cappellaro, E. 2004, *Astrophys. J.*, 607, L17
 Razzaque, S., Mészáros, P., & Waxman, E. 2003a, *Phys. Rev. Lett.*, 90, 241103
 —. 2003b, *Phys. Rev.*, D68, 083001
 —. 2004, *Phys. Rev.*, D69, 023001
 Sahu, S. & Zhang, B. 2010, *Res. Astron. Astrophys.*, 10, 943
 Schmid, J. & Turpin, D. 2016, *PoS, ICRS2015*, 1057
 Schoenen, S. & Raedel, L. 2015, *Astronomer’s Telegram* 7856
 Senno, N., Murase, K., & Mészáros, P. 2016, *Phys. Rev.*, D93, 083003
 —. 2017, arXiv:1706.02175 [astro-ph.HE]

- Sobacchi, E., Granot, J., Bromberg, O., & Sormani, M. C. 2017, *Mon. Not. Roy. Astron. Soc.*, 472, 616
- Soderberg, A. M. 2006, *AIP Conf. Proc.*, 836, 380, [,380(2006)]
- Soderberg, A. M., Frail, D. A., & Wieringa, M. H. 2004, *Astrophys. J.*, 607, L13
- Soderberg, A. M., Nakar, E., Berger, E., & Kulkarni, S. R. 2006, *ApJ*, 638, 930
- Soderberg, A. M., Nakar, E., & Kulkarni, S. R. 2006, *Astrophys. J.*, 638, 930
- Soderberg, A. M. et al. 2010, *Nature*, 463, 513
- Sonbas, E., Dhuga, K. S., Veres, P., MacLachlan, G. A., Dolek, F., Ukwatta, T. N., & Shenoy, A. 2015, *Astrophys. J.*, 805, 86
- Strolger, L.-G., Dahlen, T., Rodney, S. A., Graur, O., Riess, A. G., McCully, C., Ravindranath, S., Mobasher, B., & Shahady, A. K. 2015, *Astrophys. J.*, 813, 93
- Tamborra, I. & Ando, S. 2015, *JCAP*, 1509, 036
- . 2016, *Phys. Rev.*, D93, 053010
- Toma, K., Ioka, K., Sakamoto, T., & Nakamura, T. 2007, *Astrophys. J.*, 659, 1420
- Tomar, G., Mohanty, S., & Pakvasa, S. 2015, *JHEP*, 11, 022
- Wanderman, D. & Piran, T. 2010, *Mon. Not. Roy. Astron. Soc.*, 406, 1944
- Woosley, S. E. & Bloom, J. S. 2006, *Ann. Rev. Astron. Astrophys.*, 44, 507
- Yonetoku, D., Murakami, T., Nakamura, T., Yamazaki, R., Inoue, A. K., & Ioka, K. 2004, *Astrophys. J.*, 609, 935
- Yuksel, H., Kistler, M. D., Beacom, J. F., & Hopkins, A. M. 2008, *Astrophys. J.*, 683, L5
- Zhang, B.-B., Fan, Y.-Z., Shen, R.-F., Xu, D., Zhang, F.-W., Wei, D.-M., Burrows, D. N., & Zhang, B. 2012, *Astrophys. J.*, 756, 190

